HHS Public Access

Author manuscript

Inorg Chem. Author manuscript; available in PMC 2021 October 05.

Published in final edited form as:

Inorg Chem. 2021 June 21; 60(12): 9199–9211. doi:10.1021/acs.inorgchem.1c01269.

Tuning the Kinetic Inertness of Bi^{3+} Complexes: The Impact of Donor Atoms on Diaza-18-crown-6 Ligands as Chelators for ^{213}Bi Targeted Alpha Therapy

David J. Fiszbein[a], **Victoria Brown**[b], **Nikki A. Thiele**[a,†], **Joshua J. Woods**[a,c], **Luke Wharton**[d,e], **Samantha N. MacMillan**[a], **Valery Radchenko**[d,e], **Caterina F. Ramogida**[b,d], **Justin J. Wilson**[a,*]

[a)]Department of Chemistry and Chemical Biology, Cornell University, Ithaca, New York 14853, United States

[b)]Department of Chemistry, Simon Fraser University, 8888 University Dr, Burnaby, BC V5A 1S6 Canada

[c)]Robert F. Smith School for Chemical and Biomolecular Engineering, Cornell University, Ithaca, New York 14853, United States

[d)]Life Sciences Division, TRIUMF, 4004 Wesbrook Mall, Vancouver, BC V6T 2A3 Canada

[e)]Department of Chemistry, University of British Columbia, 2036 Main Mall, Vancouver, BC, V6T 1Z1, Canada

Abstract

The radionuclide ^{213}Bi can be applied for targeted α therapy (TAT), a type of nuclear medicine that harnesses α particles to eradicate cancer cells. To use this radionuclide for this application, a bifunctional chelator (BFC) is needed to attach it to a biological targeting vector that can deliver it selectively to cancer cells. Here, we investigated six macrocyclic ligands as potential BFCs, fully characterizing the Bi^{3+} complexes by NMR spectroscopy, mass spectrometry, and elemental analysis. Solid-state structures of three complexes revealed distorted coordination geometries about the Bi^{3+} center arising from the stereochemically active $6s^2$ lone pair. The kinetic properties of the Bi^{3+} complexes were assessed by challenging them with a 1000-fold excess of the chelating agent diethylenetriaminepentaacetic acid (DTPA). The most kinetically inert complexes contained the most basic pendent donors. Density functional theory (DFT) and quantum theory of atoms

* **Corresponding Author:** jjw275@cornell.edu .

†Present Addresses

Oak Ridge National Laboratory, Oak Ridge, Tennessee 37830, United States.

Author Contributions

The manuscript was written through contributions of all authors. All authors have given approval to the final version of the manuscript.

Supporting Information

The Supporting Information is available free of charge at https://pubs.acs.org/doi/10.1021/acs.inorgchem.1c01269.

Experimental procedures, characterization data, computational details, radiolabeling data (PDF), xyz coordinates of DFT-optimized structures (.zip)

Accession Codes

CCDC 2079740-2079742 contains the supplementary crystallographic data for this paper. These data can be obtained free of charge via www.ccdc.cam.ac.uk/data_request/cif, or by emailing data_request@ccdc.cam.ac.uk, or by contacting The Cambridge Crystallographic Data Centre, 12 Union Road, Cambridge CB2 1EZ, UK; fax: +44 1223 336033.

in molecules (QTAIM) calculations were employed to investigate this trend, suggesting that the kinetic inertness is not correlated with the extent of the $6s^2$ lone pair stereochemical activity, but with the extent of covalency between pendent donors. Lastly, radiolabeling studies of ^{213}Bi (30–210 kBq) with three of the most promising ligands showed rapid formation of the radiolabeled complexes at room temperature within 8 min for ligand concentrations as low as 10^{-7} M, corresponding to radiochemical yields of > 80% thereby demonstrating the promise of this ligand class for use in ^{213}Bi TAT.

Graphical Abstract

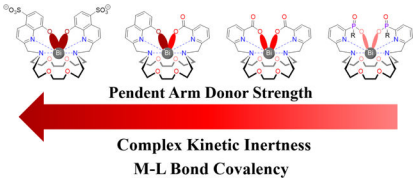

A series of 18-membered macrocyclic ligands is investigated for Bi^{3+} chelation. These ligands show promising affinity for this main group ion and are demonstrated to effectively radiolabel its therapeutic radioisotope, ^{213}Bi.

Introduction

Targeted α therapy (TAT) is a promising approach for the treatment of cancer that employs an α-emitting radionuclide to deliver highly localized internal radiation to malignant cells.[1–4] The high linear energy transfer and short penetration range in biological tissue of α particles make them well suited for internal radiotherapy because it ensures that the radiation is confined to a minimal area, thus limiting off-target damage.[5] Directing these radionuclides to malignant tissue, however, requires attachment to an appropriate biological targeting agent, such as an antibody or peptide, that can selectively bind receptors overexpressed in cancer cells (Figure 1). A key component of these radiopharmaceutical agents is the bifunctional chelator (BFC) that covalently links the α-emitting radionuclide to the targeting vector.[6] An effective BFC for radiopharmaceutical applications will form a thermodynamically stable and kinetically inert complex with the radiometal of interest within biological environments. In the context of TAT, finding a suitable BFC is hindered by the difficulty in forming stable complexes with appropriate α-emitters, which are generally isotopes of large metal ions near the bottom of the periodic table.[7] The small charge density of these large α-emitters weakens the M–L interactions that stabilize their resulting coordination complexes, requiring ligand design separate from conventional methods for smaller metal ions and limiting progress towards the utilization of TAT.

The first and currently only FDA-approved α-emitting therapeutic agent, Xofigo®, is widely employed for the management of bone metastases within castration-resistant prostate cancer patients. This drug, administered as the uncomplexed salt $[^{223}Ra]RaCl_2$,[8,9] capitalizes on the bone-mimetic properties of the free Ra^{2+} ion to localize to bone metastases.[10] Although there has been some limited success in developing chelating agents for Ra^{2+} that would enable its use for treating other cancer types,[11–15] the majority of TAT constructs under

preclinical investigation are focused on other radionuclides. Among the most promising candidates for this application are ^{225}Ac and its daughter ^{213}Bi. For example, clinical studies on a prostate-specific membrane antigen (PSMA)-targeting ^{225}Ac construct showed it to eliminate nearly all metastatic lesions in castration-resistant prostate cancer patients.[16] Despite the promising therapeutic properties of this radionuclide, there remain some concerns regarding the ability to produce it on a large enough scale with sufficiently high radionuclidic purity to sustain clinical applications.[17] The use of the daughter of ^{225}Ac, ^{213}Bi, may be advantageous in these regards as this radionuclide can conveniently be isolated from ^{225}Ac/^{213}Bi generators with high purity.[18–21] Furthermore, the shorter half-life of ^{213}Bi ($t_{1/2}$ = 45.6 min) may be favorable for some applications that involve a fast-clearing biological targeting vector and is also beneficial with respect to minimizing the redistribution of toxic daughter nuclides due to the alpha recoil effect. These promising features of ^{213}Bi have led to several clinical trials using this radionuclide for cancer treatment.[22–26]

To date, there have been numerous efforts to develop an ideal BFC for ^{213}Bi,[27–47] with varying degrees of success. Two widespread ligand design strategies for ^{213}Bi chelation focus on derivatives of the macrocyclic ligand 1,4,7,10-tetraazacyclodecane-1,4,7,10-tetraacetic acid (DOTA) and the analogue of diethylenetriaminepentaacetic acid (DTPA) with a rigidified backbone (CHX-DTPA) (Chart 1).[24,26,28,48,49] These types of ligands form ^{213}Bi complexes with good in vivo stability and high molar activities. However, macrocyclic ligands based on DOTA typically require elevated temperatures for efficient radiolabeling.[50] Furthermore, acyclic chelators, like DTPA and CHX-DTPA, tend to form less inert complexes in vivo. It should be noted, however, that CHX-DTPA shows much greater inertness compared to DTPA, a feature that has facilitated its use for in vivo studies.[22,26,48,51–55]

A common feature of both DOTA and CHX-DTPA, as well as the many other chelators that have been explored for ^{213}Bi, is their thermodynamic preference for small over large metal ions. Residing far down in the periodic table, Bi^{3+} has an ionic radius (0.96–0.99 Å for coordination number of six)[56,57] that is significantly larger than those of other +3 radiometals that have been chelated with these ligands. As such, we reasoned that investigating chelators with a reverse size-selectivity, a preference for large over small ions, would be a promising direction for the development of new BFCs for this radionuclide. In this context, ligands containing the 18-membered diaza-18-crown-6 macrocycle display this reverse size-selective property for metal ions.[58–66] Previously we have shown that macropa (Chart 1) forms remarkably stable complexes with large medicinally relevant radiometals like $^{132/135}$La, ^{223}Ra, and ^{225}Ac.[11,67,68] We have further shown that altering the pendent donor arms and macrocyclic core rigidity changes the resulting selectivity for different metal ions.[59,60,69] Based on the reverse size-selectivity properties and tunability of this system, we sought to explore this class of ligands (Chart 1) for chelating Bi^{3+} for potential applications in TAT.

Results and Discussion.

Ligand synthesis and characterization.

The ligands investigated, macropa, CHX-macropa, macropaquin, macroquin-SO_3, macrophosphi, and macrophospho (Chart 1), feature varied macrocycle rigidity and pendent donor basicity, enabling us to investigate the roles of these variables on Bi^{3+} coordination. All of these ligands, except for macrophospho, have been previously reported and were synthesized following established procedures.[58,59,69] Macrophospho, which bears two pyridyl-2-phosphonic acid pendent arms, was synthesized following an approach that was used to obtain macrophosphi (Scheme 1).[69]

The synthesis of the pendent donor arm intermediate **3** commenced from 2-(chloromethyl)pyridine-1-oxide (**2**), which could be prepared on a multigram scale in high yield by treating 2-chloromethylpyridine with *meta*-chloroperoxybenzoic acid (*m*CPBA).[70] Subsequently, the resulting pyridine-*N*-oxide **2** was activated towards an Arbuzov-type reaction[71,72] with ethyl chloroformate, and then treated in the same pot with triethyl phosphite to install the phosphonate ethyl ester. Compound **3** was isolated in 50–60% yield after sequential purification by both vacuum distillation and flash column chromatography. The alkylation of diaza-18-crown-6 with **3** in acetonitrile at reflux proceeded smoothly, resulting in the formation of **4** as a yellow oil. Compound **4**, which was carried forward in the synthesis without additional purification, was hydrolyzed with 6 M HCl to remove the ethyl ester groups. The resulting product was purified by reverse-phase preparative high-performance liquid chromatography (HPLC), and then repeatedly dissolved in 6 M HCl and concentrated to dryness under vacuum to afford macrophospho as the hydrochloride salt. This ligand was fully characterized by ^{1}H, $^{13}C\{^{1}H\}$, and $^{31}P\{^{1}H\}$ NMR spectroscopy, analytical HPLC, high-resolution mass spectrometry (HRMS), and elemental analysis (Figures S1–S6).

The protonation constants for macrophospho were determined via potentiometric titration, and are collected in Table 1, along with those for other diaza-18-crown-6-based ligands. The four most basic protonation constants of macrophospho most likely correspond to the tertiary amine nitrogens and one phosphonate oxygen on each pendent arm. We assign the two most basic protonation constants (log *K* 8.68 and 7.82) to tertiary amine nitrogens based on comparison to the analogous protonation constants for ligands such as macropa and macrophosphi, which also range from 7–8 (Table 1). A sixth protonation constant, which would belong to the last oxygen atom group, was too acidic to be measured via our potentiometric titration setup. The protonation constants of the phosphonates are lower than those of the other pendent donors, consistent with the higher acidity of this functional group. In particular, the comparison between macrophosphi and macrophospo show the that the most acidic protonation constant of the latter ligand is almost half a log unit lower. The greater acidity of phosphonates compared to phosphinates has been previously found in other ligand systems.[73]

Bi^{3+} Complex Synthesis and Characterization.

To evaluate the Bi^{3+} coordination chemistry of these ligands, we synthesized the complexes by adding $Bi(NO_3)_3{\cdot}5H_2O$ to an aqueous solution of the ligand. After 30 min of stirring at room temperature, the pH of the resulting white suspension was adjusted from ≈1.5 to 4 with 2 M KOH, and then heated at 90 °C overnight. The Bi^{3+} complexes were isolated from this reaction mixture after filtration through a 0.20 μm nylon membrane and purification by reverse-phase HPLC. Notably, the mobile phase of this purification step employed 0.1% trifluoroacetic acid (TFA), highlighting the high stabilities of the complexes under acidic conditions. All six Bi^{3+} complexes were characterized by multinuclear NMR spectroscopy, HRMS, and elemental analysis (Figures S7–S41). HRMS for all complexes revealed the presence of the characteristic *m/z* molecular ion peak for the $[M]^+$ species, and elemental analysis was consistent with the overall empirical formulae of these structures. Quantitative ^1H and ^{19}F NMR spectroscopy was used as a further verification of the average number of TFA molecules per complex. Elemental analysis and quantitative NMR methods revealed non-integer quantities of TFA molecules for some of the ligands, reflecting them to be potentially isolated as a mixture of different protonation states. The mass of TFA present in these samples was taken into consideration for subsequent studies that required precise molecular weights of these ligands.

The ^1H and $^{13}C\{^1H\}$ NMR spectra of the complexes were acquired in D_2O or DMSO-d_6 to characterize their solution properties. Coordination to the Bi^{3+} ion is confirmed by the presence of diastereotopic splitting of the methylene protons on the pendent arms and protons on the macrocyclic core. For $[Bi(macropa)]^+$, $[Bi(macrophospho)]^+$, $[Bi(macrophosphi)]^+$, and $[Bi(macroquin\text{-}SO_3)]^-$, these NMR spectra indicate that the complexes attain C_2 symmetry in solution, as reflected by the chemical equivalencies of the pendent donor groups. By contrast, $[Bi(CHX\text{-}macropa)]^+$ and $[Bi(macropaquin)]^+$ reveal asymmetric NMR spectra with discrete aromatic resonances corresponding to chemically distinct pendent donor groups (Figure 2). Distinct resonances are also observed for their associated methylenic linker protons. The lack of symmetry of these complexes suggests that the solution-state structure of all complexes involves conformations with both pendent arms on the same side of the macrocycle, similar to the solid-state structures for the Ln^{3+} and Ba^{2+} complexes.[59,67] Such a conformation has C_2 symmetry only when the pendent arms are identical, whereas different pendent arms results in a complex bearing C_1 symmetry, consistent with the NMR data.

Additionally, the NMR spectra of $[Bi(macrophosphi)]^+$ at room temperature show two species. The room temperature $^{31}P\{^1H\}$ NMR spectrum of this complex displayed three resonances in a 1:1:2 ratio (Figure 3). Upon heating this solution to 120 °C in DMSO-d_6, the peaks coalesce to a single resonance at 26.47 ppm. This 1:1:2 ratio shows three separate environments for four phosphorus atoms, consistent with the presence of a symmetric and asymmetric diastereomer of the complex with different pendent arm conformations. At elevated temperature, the interconversion of the diastereomers is rapid, resulting in coalescence of the peaks in the NMR spectra. Similarly, the $^{13}C\{^1H\}$ NMR spectrum of this complex displays three doublets for the phosphinate methyl group at room temperature that coalesce into a single doublet upon heating to 120 °C, and the aromatic region of ^1H

NMR spectrum also converges to a clean single-set of resonances at this temperature. These data corroborate our prior observations on the La^{3+} complex of this ligand.[69] Upon metal coordination, the phosphorus atoms become chiral, and thus two diastereomeric forms of the complex are possible. At higher temperatures, racemization occurs at a fast rate, giving rise to an averaged NMR spectrum.

The solid state structures of $[Bi(macropa)]^+$, $[Bi(macrophospho)]^+$, and $[Bi(macrophosphi)]^+$ were determined by X-ray diffraction (Figure 4). In contrast to their symmetric NMR spectra, these structures reveal an anisotropic coordination environment about the Bi^{3+} center. This difference between solid- and solution-state structures is most likely a consequence of stereochemical non-rigidity of the complex, which leads to time-averaged NMR spectra. The crystal structure of $[Bi(macrophosphi)]^+$ exhibits disorder about the methyl group and oxygen atom of one of the pendent phosphinate donors, reflecting the different diastereomers that were observed by NMR spectroscopy. Interatomic distances between the Bi^{3+} atom and ligand donor atoms are given in Table 2. In contrast to previously reported Lu^{3+}, La^{3+}, and Ba^{2+} crystal structures of ligands of this type, the Bi^{3+} center does not equally interact with all donors of the macrocycle. Two of the Bi–macrocycle donor interactions (Bi–N3 and Bi–O3) are significantly shorter than those between the other 4 donor atoms (N1, O2, O4). Across the three complexes, the Bi–N3 distances span values of 2.668, 2.666, and 2.659 Å, and the Bi–O3 separations are 2.7541, 2.740, and 2.669 Å for $[Bi(macropa)]^+$, $[Bi(macrophospho)]^+$, and $[Bi(macrophosphi)]^+$, respectively. The other macrocycle donor atom–Bi distances for all three complexes are greater than 2.85 Å, suggesting that only weak interactions are present. By contrast, the Bi–pendent donor atom distances are substantially shorter. The pyridyl nitrogen–Bi (Bi–N2 and Bi–N4) distances are less than 2.57 Å in all three complexes, potentially reflecting a much stronger interaction than those with the nitrogen atoms of the macrocycle. Furthermore, the Bi–O (Bi–O5 and Bi–O6) distances within all three complexes are between 2.2 and 2.3 Å, signifying a particularly strong interaction. For comparison, the Bi–O distances for the carboxylate donors within $[Bi(DTPA)]^{2-}$ and $[Bi(DOTA)]^-$ are longer at the 2.3–2.5 Å range.[74,75] Although a definitive coordination number is difficult to obtain, we propose that these structures can be best described as six-coordinate with the Bi centers displaying distorted pentagonal pyramidal geometries. Thus, the coordination environment consists of the two short Bi–macrocycle interactions, between N3 and O3, and the four Bi–pendent donor atom interactions. The pentagonal pyramidal geometry would originate from the presence of the $6s^2$ stereochemically active lone pair, which following VSEPR theory considerations, would be predicted to occupy the axial position of an ideal pentagonal bipyramid. Because a well-known impact of the stereochemically active lone pair is to shorten interatomic distances on the side opposite to it,[76] it is informative to compare the Bi–O6 and Bi–O5 separations within the three complexes. The distances between Bi and O6, the donor atom that occupies the axial position of the pentagonal pyramid, are 2.2316, 2.212, and 2.216 Å for $[Bi(macropa)]^+$, $[Bi(macrophospho)]^+$, and $[Bi(macrophosphi)]^+$, respectively, whereas the Bi–O5 distances are somewhat longer at 2.2577, 2.232. and 2.254 Å. These data therefore support our proposed pentagonal pyramidal geometry and the directionality of the stereochemically active $6s^2$ lone pair.

The SHAPE program[77] was further used to validate our assignment of the coordination polyhedra of the Bi^{3+} center for these three complexes (Table S2). Among the various ideal six-coordinate polyhedra, two geometries better matched to the experimental coordination geometries from substantially smaller continuous shape measures (CSMs). These CSMs, a quantitative measure of the match of an experimental coordination geometry to an idealized polyhedron, range from 1–4 for the Johnson pentagonal pyramid and the pentagonal pyramid. The CSMs for all other ideal polyhedra are significantly larger, on the order of 20–30, indicating that they describe the experimental geometries much more poorly. Notably, $[Bi(macropa)]^+$, $[Bi(macrophospho)]^+$, and $[Bi(macrophosphi)]^+$ have immediate coordination spheres that match the Johnson pentagonal pyramid slightly better than the pentagonal pyramid. The difference between these two geometries is the ratio of the distance of the axial vertex to the equatorial plane to the distance between two equatorial vertices, with the Johnson pentagonal pyramid having a smaller ratio. This closer match to the Johnson pentagonal pyramid is most likely due to a combination of the O6–Bi–$L_{equatorial}$ angles being less than 90° as well as the aforementioned shortened Bi–O6 bond length. Both such effects, the shortened axial bond length and contracted bond angles, support our proposal that the stereochemically active lone pair resides opposite to the axial oxygen atom.

Evaluation of the Kinetic Properties of Bi^{3+} Complexes.

To effectively use BFCs in nuclear medicine, they need to form kinetically inert complexes. To probe the kinetic inertness of each of the six Bi^{3+} complexes, we challenged them with a 1000-fold excess of the high-affinity chelator DTPA in an aqueous solution buffered at pH 7.4 with 3-(*N*-morpholino)propanesulfonic acid (MOPS). Based on the large thermodynamic affinity and significant excess of DTPA, these conditions should favor transchelation of the Bi^{3+} ion from our macrocyclic ligands to DTPA. The kinetics of this process were monitored by UV-visible spectroscopy (Figures S42–S47), allowing for the pseudo first-order half-life of this transchelation to be obtained. After spectral changes were no longer observed, the solution was analyzed by HPLC, revealing the presence of either only free ligand or the starting complex.

The half-lives measured under these conditions are collected in Table 3. Apparent from these data, the rate of transchelation varies significantly depending on the macrocyclic ligand. The most labile complexes are $[Bi(macrophospho)]^+$ and $[Bi(macrophosphi)]^+$, with dissociation half-lives of <10 and 1 min, respectively. The picolinate-bearing complexes $[Bi(CHX\text{-}macropa)]^+$ and $[Bi(macropa)]^+$ exhibit similar kinetic lability; both ligands possess half-lives near 40 min. The introduction of an 8-hydroxyquinolinate arm in the $[Bi(macropaquin)]^+$ complex increased the half-life to 14 h, marking a significant enhancement of kinetic inertness. Remarkably, $[Bi(macroquin\text{-}SO_3)]^-$, which contains two 8-hydroxyquinolinate-based pendent arms, does not show any spectral changes over a 21-d time period, demonstrating excellent kinetic inertness.

In comparing $[Bi(CHX\text{-}macropa)]^+$ and $[Bi(macropa)]^+$, which exhibit nearly identical decomplexation half-lives, the rigidity of the macrocycle does not significantly influence the complex inertness towards the DTPA challenges. By contrast, more significant inertness manifests with increasing pendent donor basicity. Macrophospho and macrophosphi, which

possess the least basic pendent arms (oxygen donor pK_a values of < 2), form the most labile complexes with Bi^{3+}, whereas the ligands with the significantly more basic quinolinate donors, macropaquin and macroquin-SO_3 (oxygen donor pK_a values of 9–10), demonstrate the highest levels of kinetic inertness. Macropa and CHX-macropa, bearing carboxylate oxygen donors (pK_a values of 2–3), show intermediate levels of kinetic inertness. The efficacy of macropaquin and macroquin-SO_3 for stabilizing Bi^{3+} in this DTPA challenge contrasts our observations with other large labile metal ions. For example, macroquin-SO_3 was previously found to be the poorest candidate for retaining Ba^{2+} under similar challenge conditions, whereas macropa was the most effective.[59] Furthermore, the La^{3+} complex of macropa is kinetically inert for over 20 d when treated with DTPA under similar conditions.[67] Considering that Bi^{3+} and La^{3+} have similar ionic radii, the relative lability of the $[Bi(macropa)]^+$ complex is surprising and points to additional factors that are required to stabilize this main group ion.

Computational Studies.

The origin of the differing kinetic properties of these complexes was investigated using density functional theory (DFT) calculations at the TPSSh level of theory.[78] The Bi^{3+} atom was treated with the large core relativistic effective core potential (ECP60MDF)[79] and related basis set, and the ligand atoms were described using the triple zeta valence potential (TZVP) basis set.[80] We selected this computational approach based on previous studies that have demonstrated that this functional and effective core potential combination yield good results for Bi^{3+} complexes.[39,46] Upon optimization, all six geometries converged to local minima with significant structural distortions about the central Bi^{3+} ion due to the presence of the stereochemically active lone pair. Notably, the DFT-optimized structures of $[Bi(macropa)]^+$, $[Bi(macrophospho)]^+$, and $[Bi(macrophosphi)]^+$ compare favorably to those determined experimentally by X-ray crystallography with root-mean square differences (RMSDs) between these structures of 0.144, 0.218, and 0.233 Å, respectively. As discussed above, the Bi^{3+} complex of macropa is significantly less inert than those of macropaquin and macroquin-SO_3, which is in contrast to that of the highly inert La^{3+} complex of macropa. We hypothesized that the stereochemical activity of the $6s^2$ lone pair in the Bi^{3+} complexes, a feature that is not present within the La^{3+} complex, may affect their relative kinetic labilities. The degree of stereochemical activity of the Bi^{3+} lone pair is a result of mixing between the 6s and 6p orbitals, which perturbs the spherical distribution of the 6s shell.[81] The degree of 6p mixing was analyzed using a Natural Bond Orbital (NBO) analysis, which has proven useful for calculations dealing with stereochemical activity of the lone pair in Bi^{3+} and Pb^{2+} complexes.[46,63,76,82–84] Each complex contains 1–2% 6p character, which agrees well with previous calculations on similar complexes (Table 4).[46,84] Contour plots of the electron density of the molecular orbitals (MOs) containing significant (15–20%) Bi $6s^2$ contribution show that the lone pair extends away from the Bi^{3+} nucleus and towards the macrocyclic core (Figure 5). Contrary to our hypothesis, however, there is not a distinctive trend between the degree of 6p contribution and the kinetic lability of the Bi^{3+} complex (Table 3). This result suggests that the stereochemical activity of the lone pair is not the sole source of the differing kinetic labilities of these macrocyclic chelators with Bi.

To further investigate the origin of the differing complex kinetic properties, we employed Bader's quantum theory of atoms in molecules (QTAIM) analysis.[85] This technique probes the topology of the electron density of complexes and has been used with great success to understand bonding in metal complexes.[86,87] Within the QTAIM framework, the electron density, $\rho(r)$, is divided into partitions represented by zero-flux surfaces, with the bond path between two atoms defined by the line of local maximum density. The intersection of the bond path and the zero-flux surface is defined as the bond critical point (BCP). Properties at the BCP, such as the electron density $\rho(r)$, Laplacian of the electron density $\nabla^2\rho(r)$, Lagrangian kinetic energy G(r), potential energy V(r), total energy density H(r), and delocalization index δ, describe the nature of the chemical interaction between two atoms. In the case of heavy elements, such as Bi, the $\nabla^2\rho(r)$ may not properly describe the nature of metal-ligand bonding interactions.[88,89] To avoid this issue, the energy density parameters V(r), G(r), and H(r), the ratio of potential and kinetic energies |V|/G, and the normalized total energy density H/ρ are commonly used to interpret the nature of bonding interactions in heavy metal complexes.[90–95]

Complete QTAIM results are compiled in Tables 5 and S3–S8. In agreement with our X-ray crystallographic and NBO analysis, the interactions of the Bi^{3+} center with the crown ether oxygen (O1–O4) and amine nitrogen (N1 and N3) atoms of the diaza-18-crown-6 core are almost purely ionic nature, as evidenced by the values of $H(r) \geq 0$ and $|V|/G < 1$ (Table S3–S8). The interatomic interactions between the Bi center and the donor atoms of the pendent arms (O5, O6, N2, and N4) are more covalent, with values of $H(r) < 0$ and $|V|/G > 1$. The degree of covalency in these bonds can be analyzed by comparing the magnitude of the normalized energy density (H/ρ). Increased covalent character is reflected by more negative values of this parameter.[91,92,96,97] As seen in Table 5, the covalency of the Bi–O and Bi–N bonds increases with the ligand basicity and agrees well with the trend in experimental kinetic properties of the chelators. A similar trend is observed for δ, which is an integral property that can be considered as a measure of covalent bond order.[81,98]

A recent study has shown that topological analysis of QTAIM parameters along the length of the bond path, rather than just at the BCP, provides useful information into the nature of the bonding interactions in complexes containing heavy main-group elements.[99] As such, we evaluated ρ and $\nabla^2\rho(r)$ across the entire length of the Bi–O bonds in $[Bi(macrophosphi)]^+$ and $[Bi(macroquin\text{-}SO_3)]^-$. To account for differing interatomic distances and facilitate comparison of the complexes, the interatomic distances were normalized to one-unit length. The plot of $\rho(r)$ reveals a clear minimum between the atoms, indicating the location of the BCP for the Bi–O interaction (Figure 6a). For both complexes, the BCP is shifted away from the midpoint of the bond path and towards the oxygen atom, which highlights the different electronegativities of the elements and the polarized nature of this interaction. The BCP is less shifted from the midpoint of the Bi and O atoms for $[Bi(macroquin\text{-}SO_3)]^-$ compared to $[Bi(macrophosphi)]^+$, which suggests that the distribution of $\rho(r)$ across the bond is slightly more symmetric and the interaction is more covalent in nature. This result agrees with the analysis of the energy density parameters at the BCP (Table 5). In the plot of $\nabla^2\rho(r)$, the single local minimum along the bond path is located near the oxygen atom (Figure 6b), a feature that is observed in other systems with interactions between second-period elements and third- and fourth-period elements.[99–104] It has been shown that

the decrease in the magnitude of this local minimum can be attributed to a decrease in bond order.[99] As expected, the local minimum for $[Bi(macroquin\text{-}SO_3)]^-$ is considerably more negative than for $[Bi(macroposphi)]^+$, suggesting that the interaction between Bi and the O donor atoms of the quinoline pendent arms is more covalent in nature than those of the picolinate donors. Taken together, these results suggest that the enhanced kinetic inertness of $[Bi(macroquin\text{-}SO_3)]^-$ compared to the other chelators described here may stem from the increased covalency between the metal center and the donor atoms of the pendent arms.

Radiolabeling Studies.

As a final validation on the value of these chelators for ^{213}Bi TAT, we carried out radiolabeling studies using macropa, macropaquin, and macroquin-SO_3, which formed comparatively more inert Bi^{3+} complexes than the other ligands. These ligands, in concentrations ranging from 10^{-7} to 10^{-4} M, were mixed with $[^{213}Bi]BiI_4^-$/$[^{213}Bi]BiI_5^{2-}$ (30 kBq–210 kBq), freshly eluted from a ^{225}Ac/^{213}Bi generator, in pH 5.5 2-(*N*-morpholino)ethanesulfonic acid (MES) buffer. As radiolabeling progressed at room temperature for 18-membered macrocycles or 95 °C for DOTA, aliquots were removed and analyzed by radio-TLC to assess the radiochemical yields (RCYs) after 8 min for 18-membered macrocycles or 5.5 min for DOTA. The resulting concentration-dependent RCYs for each ligand are collected in Table 6 and Figure 7. Notably, despite the radiolabeling reactions being performed at room temperature for the 18-membered macrocycles, the RCYs obtained are greater than those for DOTA, which required heating at 95 °C for all concentrations. At the highest ligand concentration (10^{-4} M), macropa, macropaquin, and DOTA quantitatively radiolabel ^{213}Bi, whereas macroquin-SO_3 achieved a 91% RCY under these conditions. For all four ligands, RCYs of approximately 90% are maintained upon decreasing the ligand concentration by two order of magnitude to 10^{-6} M. At ligand concentrations of 10^{-7} M, significant differences in the RCYs are observed across the four chelators. DOTA and macropaquin perform the poorest at this concentration, reaching RCYs of approximately 12 and 15%, respectively. Macroquin-SO_3 achieves a moderate 40% RCY at this concentration, whereas macropa maintains a RCY of approximately 80%, affirming its superior radiolabeling capabilities. Notably, all three of these macrocyclic ligands outperform DOTA, indicating that they may be more favorable for use in ^{213}Bi TAT.

A comparison of the radiolabeling properties of these ligands can also be discerned from the decay-corrected molar activities (Table 7). At the lowest ligand concentrations required to achieve > 80% RCY, molar activities of 8.69, 1.49, and 1.82 MBq/nmol were obtained for the radiolabeled complexes of macropa, macropaquin, and macroquin-SO_3, respectively. These values are significantly larger than the molar activity of 0.284 MBq/mol that was achieved with DOTA under elevated temperatures. In particular, the 30-fold greater molar activity of macropa in comparison to DOTA, which was accomplished at room temperature, highlights the effective ^{213}Bi-radiolabeling properties of these 18-membered macrocycles.

Conclusions

In conclusion, a set of six macrocyclic ligands were evaluated for their potential as Bi^{3+} chelators in TAT. These ligands, all containing the 18-membered diaza-18-crown-6

macrocyclic core, differed based on their pendent donors, as well as macrocycle rigidity. The evaluation of the kinetic properties of the Bi^{3+} complexes revealed that macrocycle rigidity had little influence on their inertness, in contrast to pendent donor basicity, which played a large role. Specifically, more basic donors, like the quinolinate groups found in macroquin-SO_3, gave rise to more kinetically inert complexes, whereas the least basic phosphinate and phosphonate groups yielded labile complexes. To understand the origins of this effect, the complexes were fully characterized by solid-state and solution methods. Although the solid-state X-ray crystal structures showed profound structural distortion arising from the stereochemically active $6s^2$ lone pair of the Bi^{3+} ion, NMR studies indicate that an averaged symmetric complex is obtained in solution. Furthermore, DFT calculations verified that the extent of the stereochemical activity of this lone pair, as measured by the corresponding %p character, had little ramifications on the overall inertness of the complexes. By contrast, these computational studies predicted that an increase in covalency contributed to the enhanced inertness of the macroquin-SO_3 complex over those of the other ligands. Despite the excellent kinetic inertness of the $[Bi(\text{macroquin-}SO_3)]^-$ complex, radiolabeling of this ligand with ^{213}Bi was relatively inefficient compared to macropa. Given the short half-life of ^{213}Bi, the faster radiolabeling and higher molar activities afforded by macropa may be more favorable for applications in TAT.

In summary, this study has shown that the diaza-18-crown-6 scaffold is highly promising for use in Bi^{3+} chelation, displaying several advantages, such as vast tunability and rapid complex formation, over the conventional cyclen-based chelators. The tunability of this class of ligands via changing the basicity of the pendent donor groups can be valuable for accessing new highly promising BFCs for ^{213}Bi TAT. Future work will assess the suitability of the ligands in this study for this application.

Supplementary Material

Refer to Web version on PubMed Central for supplementary material.

Funding Sources

This research was supported by funding from the College of Arts and Sciences at Cornell University, by the National Institute for Biomedical Imaging and Bioengineering of the National Institutes of Health under award number R01 EB029259, and by the Research Corporation for Science Advancement in the form of a Cottrell Scholar Award to J. J. Wilson. J. J. Woods thanks the American Heart Association for a predoctoral fellowship (20PRE35120390). This research also made use of the NMR Facility at Cornell University, which is supported, in part, by the United States National Science Foundation under Award CHE-1531632. We gratefully acknowledge the Natural Sciences and Engineering Research Council (NSERC) of Canada for a CREATE IsoSiM at TRIUMF research stipend (L. Wharton), financial support via NSERC Discovery Grants (V. Radchenko), and support via a Master's Canada Graduate Scholarship (V. Brown). TRIUMF receives federal funding via a contribution agreement with the National Research Council of Canada.

REFERENCES

(1). Kim Y-SS; Brechbiel MWAn Overview of Targeted Alpha Therapy. Tumor Biol. 2012, 33, 573–590.

(2). Dekempeneer Y; Keyaerts M; Krasniqi A; Puttemans J; Muyldermans S; Lahoutte T; D'huyvetter M; Devoogdt NTargeted Alpha Therapy Using Short-Lived Alpha-Particles and the Promise of Nanobodies as Targeting Vehicle. Expert Opin. Biol. Ther2016, 16, 1035–1047. [PubMed: 27145158]

(3). Couturier O; Supiot S; Degraef-Mougin M; Faivre-Chauvet A; Carlier T; Chatal J-F; Davodeau F; Cherel MCancer Radioimmunotherapy with Alpha-Emitting Nuclides. Eur. J. Nucl. Med. Mol. Imaging2005, 32, 601–614. [PubMed: 15841373]

(4). Brechbiel MWTargeted α-Therapy: Past, Present, Future?Dalton Trans. 2007, 4918–4928. [PubMed: 17992276]

(5). Mulford DA; Scheinberg DA; Jurcic JGThe Promise of Targeted α-Particle Therapy. J. Nucl. Med2005, 46, 199S–204S. [PubMed: 15653670]

(6). Price EW; Orvig CMatching Chelators to Radiometals for Radiopharmaceuticals. Chem. Soc. Rev2014, 43, 260–290. [PubMed: 24173525]

(7). Kostelnik TI; Orvig CRadioactive Main Group and Rare Earth Metals for Imaging and Therapy. Chem. Rev2019, 119, 902–956. [PubMed: 30379537]

(8). Harrison MR; Wong TZ; Armstrong AJ; George DJRadium-223 Chloride: A Potential New Treatment for Castration-Resistant Prostate Cancer Patients with Metastatic Bone Disease. Cancer Manag. Res2013, 5, 1–14. [PubMed: 23326203]

(9). Pandit-Taskar N; Larson SM; Carrasquillo JABone-Seeking Radiopharmaceuticals for Treatment of Osseous Metastases, Part 1: α Therapy with ^{223}Ra-Dichloride. J. Nucl. Med2014, 55, 268–274. [PubMed: 24343987]

(10). Coleman RTreatment of Metastatic Bone Disease and the Emerging Role of Radium-223. Semin. Nucl. Med2016, 46, 99–104. [PubMed: 26897713]

(11). Abou DS; Thiele NA; Gutsche NT; Villmer A; Zhang H; Woods JJ; Baidoo KE; Escorcia FE; Wilson JJ; Thorek DLJTowards the Stable Chelation of Radium for Biomedical Applications with an 18-Membered Macrocyclic Ligand. Chem. Sci2021, 12, 3733–3742. [PubMed: 34163647]

(12). Matyskin AV; Hansson NL; Brown PL; Ekberg CBarium and Radium Complexation with Ethylenediaminetetraacetic Acid in Aqueous Alkaline Sodium Chloride Media. J. Solution Chem2017, 46, 1951–1969. [PubMed: 29187768]

(13). Chiarizia R; Horwitz EP; Dietz ML; Cheng YDRadium Separation through Complexation by Aqueous Crown Ethers and Extraction by Dinonylnaphthalenesulfonic Acid. React. Funct. Polym1998, 38, 249–257.

(14). Henriksen G; Hoff P; Larsen RHEvaluation of Potential Chelating Agents for Radium. Appl. Radiat. Isot2002, 56, 667–671. [PubMed: 11993940]

(15). Chen X; Ji M; Fisher DR; Wai CMIonizable Calixarene-Crown Ethers with High Selectivity for Radium over Light Alkaline Earth Metal Ions. Inorg. Chem1999, 38, 5449–5452.

(16). Kratochwil C; Bruchertseifer F; Giesel FL; Weis M; Verburg FA; Mottaghy F; Kopka K; Apostolidis C; Haberkorn U; Morgenstern A^{225}Ac-PSMA-617 for PSMA-Targeted α-Radiation Therapy of Metastatic Castration-Resistant Prostate Cancer. J. Nucl. Med2016, 57, 1941–1944. [PubMed: 27390158]

(17). Morgenstern A; Apostolidis C; Bruchertseifer FSupply and Clinical Application of Actinium-225 and Bismuth-213. Semin. Nucl. Med2020, 50, 119–123. [PubMed: 32172796]

(18). Guseva LI; Dogadkin NNA Generator System for Production of Medical Alpha-Radionuclides Ac-225 and Bi-213. J. Radioanal. Nucl. Chem2010, 285, 667–673.

(19). Morgenstern A; Bruchertseifer F; Apostolidis CBismuth-213 and Actinium-225 – Generator Performance and Evolving Therapeutic Applications of Two Generator-Derived Alpha-Emitting Radioisotopes. Curr. Radiopharm2012, 5, 221–227. [PubMed: 22642390]

(20). Bond AH; Rogers RDBismuth Coordination Chemistry: A Brief Retrospective Spanning Crystallography to Clinical Potential. J. Coord. Chem2021, 74, 129–151.

(21). McDevitt MR; Finn RD; Sgouros G; Ma D; Scheinberg DAAn ^{225}Ac/^{213}Bi Generator System for Therapeutic Clinical Applications : Construction and Operation. Appl. Radiat. Isot1999, 50, 895–904. [PubMed: 10214708]

(22). Jurcic JG; Larson SM; Sgouros G; McDevitt MR; Finn RD; Divgi CR; Ballangrud ÅM; Hamacher KA; Ma D; Humm JL; Brechbiel MW; Molinet R; Scheinberg DATargeted α Particle Immunotherapy for Myeloid Leukemia. Blood2002, 100, 1233–1239. [PubMed: 12149203]

(23). Kneifel S; Cordier D; Good S; Ionescu MCS; Ghaffari A; Hofer S; Kretzschmar M; Tolnay M; Apostolidis C; Waser B; Arnold M; Mueller-Brand J; Maecke HR; Reubi

JC; Merlo ALocal Targeting of Malignant Gliomas by the Diffusible Peptidic Vector 1,4,7,10-Tetraazacyclododecane-1-Glutaric Acid-4,7,10-Triacetic Acid-Substance P. Clin. Cancer Res2006, 12, 3843–3850. [PubMed: 16778112]

(24). Cordier D; Forrer F; Bruchertseifer F; Morgenstern A; Apostolidis C; Good S; Müller-Brand J; Mäcke H; Reubi JC; Merlo ATargeted Alpha-Radionuclide Therapy of Functionally Critically Located Gliomas with ^{213}Bi-DOTA-[Thi^{8},Met(O_2)^{11}]- Substance P: A Pilot Trial. Eur. J. Nucl. Med. Mol. Imaging2010, 37, 1335–1344. [PubMed: 20157707]

(25). Raja C; Graham P; Abbas Rizvi SM; Song E; Goldsmith H; Thompson J; Bosserhoff A; Morgenstern A; Apostolidis C; Kearsley J; Reisfeld R; Allen BJInterim Analysis of Toxicity and Response in Phase 1 Trial of Systemic Targeted Alpha Therapy for Metastatic Melanoma. Cancer Biol. Ther2007, 6, 846–852. [PubMed: 17495524]

(26). Rosenblat TL; McDevitt MR; Mulford DA; Pandit-Taskar N; Divgi CR; Panageas KS; Heaney ML; Chanel S; Morgenstern A; Sgouros G; Larson SM; Scheinberg DA; Jurcic JGSequential Cytarabine and α-Particle Immunotherapy with Bismuth-213-Lintuzumab (HuM195) for Acute Myeloid Leukemia. Clin. Cancer Res2010, 16, 5303–5311. [PubMed: 20858843]

(27). Egorova BV; Matazova EV; Mitrofanov AA; Aleshin GY; Trigub AL; Zubenko AD; Fedorova OA; Fedorov YV; Kalmykov SNNovel Pyridine-Containing Azacrownethers for the Chelation of Therapeutic Bismuth Radioisotopes: Complexation Study, Radiolabeling, Serum Stability and Biodistribution. Nucl. Med. Biol2018, 60, 1–10. [PubMed: 29499420]

(28). Wilson JJ; Ferrier M; Radchenko V; Maassen JR; Engle JW; Batista ER; Martin RL; Nortier FM; Fassbender ME; John KD; Birnbaum EREvaluation of Nitrogen-Rich Macrocyclic Ligands for the Chelation of Therapeutic Bismuth Radioisotopes. Nucl. Med. Biol2015, 42, 428–438. [PubMed: 25684650]

(29). Šimeček J; Hermann P; Seidl C; Bruchertseifer F; Morgenstern A; Wester H-J; Notni JEfficient Formation of Inert Bi-213 Chelates by Tetraphosphorus Acid Analogues of DOTA: Towards Improved Alpha-Therapeutics. EJNMMI Res. 2018, 8, 78. [PubMed: 30091088]

(30). Briand GG; Burford NBismuth Compounds and Preparations with Biological or Medicinal Relevance. Chem. Rev1999, 99, 2601–2657. [PubMed: 11749495]

(31). Hassfjell S; Brechbiel MWThe Development of the α-Particle Emitting Radionuclides ^{212}Bi and ^{213}Bi, and Their Decay Chain Related Radionuclides, for Therapeutic Applications. Chem. Rev2001, 101, 2019–2036. [PubMed: 11710239]

(32). Stavila V; Davidovich RL; Gulea A; Whitmire KHBismuth(III) Complexes with Aminopolycarboxylate and Polyaminopolycarboxylate Ligands: Chemistry and Structure. Coord. Chem. Rev2006, 250, 2782–2810.

(33). Sinenko IL; Kalmykova TP; Likhosherstova DV; Egorova BV; Zubenko AD; Vasiliev AN; Ermolaev SV; Lapshina EV; Ostapenko VS; Fedorova OA; Kalmykov SN^{213}Bi Production and Complexation with New Picolinate Containing Ligands. J. Radioanal. Nucl. Chem2019, 321, 531–540.

(34). Matazova EV; Egorova BV; Konopkina EA; Aleshin GY; Zubenko AD; Mitrofanov AA; Karpov KV; Fedorova OA; Fedorov YV; Kalmykov SNBenzoazacrown Compound: A Highly Effective Chelator for Therapeutic Bismuth Radioisotopes. MedChemComm2019, 10, 1641–1645. [PubMed: 31814957]

(35). Lange JL; Davey PRWJ; Ma MT; White JM; Morgenstern A; Bruchertseifer F; Blower PJ; Paterson BMAn Octadentate Bis(Semicarbazone) Macrocycle: A Potential Chelator for Lead and Bismuth Radiopharmaceuticals. Dalton Trans. 2020, 49, 14962–14974. [PubMed: 33079111]

(36). Dadwal M; Kang CS; Song HA; Sun X; Dai A; Baidoo KE; Brechbiel MW; Chong H-SSynthesis and Evaluation of a Bifunctional Chelate for Development of Bi(III)-Labeled Radioimmunoconjugates. Bioorg. Med. Chem. Lett2011, 21, 7513–7515. [PubMed: 22047687]

(37). Chong H-S; Lim S; Baidoo KE; Milenic DE; Ma X; Jia F; Song HA; Brechbiel MW; Lewis MRSynthesis and Biological Evaluation of a Novel Decadentate Ligand DEPA. Bioorg. Med. Chem. Lett2008, 18, 5792–5795. [PubMed: 18845437]

(38). Chong H-S; Song HA; Birch N; Le T; Lim S; Ma XEfficient Synthesis and Evaluation of Bimodal Ligand NETA. Bioorg. Med. Chem. Lett2008, 18, 3436–3439. [PubMed: 18445528]

(39). Lima LMP; Beyler M; Delgado R; Platas-Iglesias C; Tripier RInvestigating the Complexation of the Pb^{2+}/Bi^{3+} Pair with Dipicolinate Cyclen Ligands. Inorg. Chem2015, 54, 7045–7057. [PubMed: 26146022]

(40). Thiabaud G; Radchenko V; Wilson JJ; John KD; Birnbaum ER; Sessler JLRapid Insertion of Bismuth Radioactive Isotopes into Texaphyrin in Aqueous Media. J. Porphyrins Phthalocyanines2017, 21, 882–886.

(41). Lima LMP; Beyler M; Oukhatar F; Le Saec P; Faivre-Chauvet A; Platas-Iglesias C; Delgado R; Tripier RH_2Me-Do2pa: An Attractive Chelator with Fast, Stable and Inert $^{nat}Bi^{3+}$ and $^{213}Bi^{3+}$ Complexation for Potential α-Radioimmunotherapy Applications. Chem. Commun2014, 50, 12371–12374.

(42). Brechbiel MW; Gansow OA; Pippin CG; Rogers RD; Planalp RPPreparation of the Novel Chelating Agent *N*-(2-Aminoethyl)-*trans*-1,2-Diaminocyclohexane-*N*,*N*′,*N*″-Pentaacetic Acid (H_5CyDTPA), a Preorganized Analogue of Diethylenetriaminepentaacetic Acid (H_5DTPA), and the Structure of $Bi^{III}(CyDTPA)^{2-}$ and $Bi^{III}(H_2DTPA)$ Complexes. Inorg. Chem1996, 35, 6343–6348.

(43). Kozak RW; Waldmann TA; Atcher RW; Gansow OARadionuclide-Conjugated Monoclonal Antibodies: A Synthesis of Immunology, Inorganic Chemistry and Nuclear Science. Trends Biotechnol. 1986, 4, 259–264.

(44). Chong H-S; Milenic DE; Garmestani K; Brady ED; Arora H; Pfiester C; Brechbiel MWIn vitro and in vivo Evaluation of Novel Ligands for Radioimmunotherapy. Nucl. Med. Biol2006, 33, 459–467. [PubMed: 16720237]

(45). Hassfjell S; Kongshaug KO; Romming CSynthesis, Crystal Structure and Chemical Stability of Bismuth(III) Complexed with 1,4,7,10-Tetraazacyclododecane-1,4,7,10-Tetramethylene Phosphonic Acid (H_8DOTMP). Dalton Trans. 2003, 1433–1437.

(46). Pujales-Paradela R; Rodríguez-Rodríguez A; Gayoso-Padula A; Brandariz I; Valencia L; Esteban-Gómez D; Platas-Iglesias COn the Consequences of the Stereochemical Activity of the Bi(III) $6s^2$ Lone Pair in Cyclen-Based Complexes. the [Bi(DO3A)] Case. Dalton Trans. 2018, 47, 13830–13842. [PubMed: 30230496]

(47). Bruchertseifer F; Comba P; Martin B; Morgenstern A; Notni J; Starke M; Wadepohl HFirst-Generation Bispidine Chelators for $^{213}Bi^{III}$ Radiopharmaceutical Applications. ChemMedChem2020, 15, 1591–1600. [PubMed: 32613737]

(48). Milenic DE; Roselli M; Mirzadeh S; Pippin CG; Gansow OA; Colcher D; Brechbiel MW; Schlom JIn vivo Evaluation of Bismuth-Labeled Monoclonal Antibody Comparing DTPA-Derived Bifunctional Chelates. Cancer Biother. Radiopharm2001, 16, 133–146. [PubMed: 11385960]

(49). Montavon G; Le Du A; Champion J; Rabung T; Morgenstern ADTPA Complexation of Bismuth in Human Blood Serum. Dalton Trans. 2012, 41, 8615–8623. [PubMed: 22678751]

(50). Chan HS; de Blois E; Konijnenberg MW; Morgenstern A; Bruchertseifer F; Norenberg JP; Verzijlbergen FJ; de Jong M; Breeman WAPOptimizing Labelling Conditions of ^{213}Bi-DOTATATE for Preclinical Applications of Peptide Receptor Targeted Alpha Therapy. EJNMMI Radiopharm. Chem2016, 1, 9. [PubMed: 29564386]

(51). Fazel J; Rötzer S; Seidl C; Feuerecker B; Autenrieth M; Weirich G; Bruchertseifer F; Morgenstern A; Senekowitsch-Schmidtke RFractionated Intravesical Radioimmunotherapy with ^{213}Bi-Anti-EGFR-MAb Is Effective without Toxic Side-Effects in a Nude Mouse Model of Advanced Human Bladder Carcinoma. Cancer Biol. Ther2015, 16, 1526–1534. [PubMed: 26177233]

(52). Teiluf K; Seidl C; Blechert B; Gaertner FC; Gilbertz K-P; Fernandez V; Bassermann F; Endell J; Boxhammer R; Leclair S; Vallon M; Aichler M; Feuchtinger A; Bruchertseifer F; Morgenstern A; Essler Mα-Radioimmunotherapy with ^{213}Bi-Anti-CD38 Immunoconjugates Is Effective in a Mouse Model of Human Multiple Myeloma. Oncotarget2015, 6, 4692–4703. [PubMed: 25576914]

(53). Fichou N; Gouard S; Maurel C; Barbet J; Ferrer L; Morgenstern A; Bruchertseifer F; Faivre-Chauvet A; Bigot-Corbel E; Davodeau F; Gaschet J; Chérel MSingle-Dose Anti-CD138 Radioimmunotherapy: Bismuth-213 Is More Efficient than Lutetium-177 for Treatment of Multiple Myeloma in a Preclinical Model. Front. Med2015, 2, 76.

(54). Senekowitsch-Schmidtke R; Schuhmacher C; Becker K-F; Nikula TK; Seidl C; Becker I; Miederer M; Apostolidis C; Adam C; Huber R; Kremmer E; Fischer K; Schwaiger MHighly Specific Tumor Binding of a ^{213}Bi-Labeled Monoclonal Antibody against Mutant E-Cadherin Suggests Its Usefulness for Locoregional α-Radioimmunotherapy of Diffuse-Type Gastric Cancer. Cancer Res. 2001, 61, 2804–2808. [PubMed: 11306447]

(55). Friesen C; Glatting G; Koop B; Schwarz K; Morgenstern A; Apostolidis C; Debatin K-M; Reske SNBreaking Chemoresistance and Radioresistance with [^{213}Bi]Anti- CD45 Antibodies in Leukemia Cells. Cancer Res. 2007, 67, 1950–1958. [PubMed: 17332322]

(56). Shannon RDRevised Effective Ionic Radii and Systematic Studies of Interatomic Distances in Halides and Chalcogenides. Acta Crystallogr., Sect. A: Found. Adv1976, 32, 751–767.

(57). Näslund J; Persson I; Sandström MSolvation of the Bismuth(III) Ion by Water, Dimethyl Sulfoxide, *N,N'*-Dimethylpropyleneurea, and *N,N*-Dimethylthioformamide. An EXAFS, Large-Angle X-Ray Scattering, and Crystallographic Structural Study. Inorg. Chem2000, 39, 4012–4021. [PubMed: 11198855]

(58). Roca-Sabio A; Mato-Iglesias M; Esteban-Gómez D; Tóth É; De Bias A; Platas-Iglesias C; Rodríguez-Blas TMacrocyclic Receptor Exhibiting Unprecedented Selectivity for Light Lanthanides. J. Am. Chem. Soc2009, 131, 3331–3341. [PubMed: 19256570]

(59). Thiele NA; MacMillan SN; Wilson JJRapid Dissolution of $BaSO_4$ by Macropa, an 18-Membered Macrocycle with High Affinity for Ba^{2+}. J. Am. Chem. Soc2018, 140, 17071–17078. [PubMed: 30485079]

(60). Thiele NA; Woods JJ; Wilson JJImplementing f-Block Metal Ions in Medicine: Tuning the Size Selectivity of Expanded Macrocycles. Inorg. Chem2019, 58, 10483–10500. [PubMed: 31246017]

(61). Carreira-Barral I; Rodríguez-Rodríguez A; Regueiro-Figueroa M; Esteban-Gómez D; Platas-Iglesias C; de Blas A; Rodríguez-Blas TA Merged Experimental and Theoretical Conformational Study on Alkaline-Earth Complexes with Lariat Ethers Derived from 4,13-Diaza-18-Crown-6. Inorg. Chim. Acta2011, 370, 270–278.

(62). Jensen MP; Chiarizia R; Shkrob IA; Ulicki JS; Spindler BD; Murphy DJ; Hossain M; Roca-Sabio A; Platas-Iglesias C; de Blas A; Rodríguez-Blas TAqueous Complexes for Efficient Size-Based Separation of Americium from Curium. Inorg. Chem2014, 53, 6003–6012. [PubMed: 24890863]

(63). Ferreirós-Martínez R; Esteban-Gómez D; Tóth É; de Blas A; Platas-Iglesias C; Rodríguez-Blas TMacrocyclic Receptor Showing Extremely High Sr(II)/Ca(II) and Pb(II)/Ca(II) Selectivities with Potential Application in Chelation Treatment of Metal Intoxication. Inorg. Chem2011, 50, 3772–3784. [PubMed: 21413756]

(64). Chang CA; Rowland MEMetal Complex Formation with 1,10- Diaza-4,7,13,16-Tetraoxacyclooctadecane-*N,N'* -Diacetic Acid. An Approach to Potential Lanthanide Ion Selective Reagents. Inorg. Chem1983, 22, 3866–3869.

(65). Brücher E; Györi B; Emri J; Solymosi P; Sztanyik LB; Varga L1,10-Diaza-4,7,13,16-Tetraoxacyclooctadecane-1,10-Bis(Malonate), a Ligand with High Sr^{2+}/Ca^{2+} and Pb^{2+}/Zn^{2+} Selectivities in Aqueous Solution. J. Chem. Soc., Chem. Commun1993, 574–575.

(66). Peters JA; Djanashvili K; Geraldes CFGC; Platas-Iglesias CThe Chemical Consequences of the Gradual Decrease of the Ionic Radius along the Ln-Series. Coord. Chem. Rev2020, 406, 213146.

(67). Thiele NA; Brown V; Kelly JM; Amor-Coarasa A; Jermilova U; MacMillan SN; Nikolopoulou A; Ponnala S; Ramogida CF; Robertson AKH; Rodríguez-Rodríguez C; Schaffer P; Williams C Jr.; Babich JW; Radchenko V; Wilson JJAn Eighteen-Membered Macrocyclic Ligand for Actinium-225 Targeted Alpha Therapy. Angew. Chem., Int. Ed2017, 56, 14712–14717.

(68). Aluicio-Sarduy E; Thiele NA; Martin KE; Vaughn BA; Devaraj J; Olson AP; Barnhart TE; Wilson JJ; Boros E; Engle JWEstablishing Radiolanthanum Chemistry for Targeted Nuclear Medicine Applications. Chem. - Eur. J2020, 26, 1238–1242. [PubMed: 31743504]

(69). Thiele NA; Fiszbein DJ; Woods JJ; Wilson JJTuning the Separation of Light Lanthanides Using a Reverse-Size Selective Aqueous Complexant. Inorg. Chem2020, 59, 16522–16530. [PubMed: 33103417]

(70). Polášek M; Šedinová M; Kotek J; Vander Elst L; Muller RN; Hermann P; Lukeš IPyridine-*N*-Oxide Analogues of DOTA and Their Gadolinium(III) Complexes Endowed with a Fast

Water Exchange on the Square-Antiprismatic Isomer. Inorg. Chem2009, 48, 455–465. [PubMed: 19090686]

(71). Lee S-J; Kim H-S; Yang H-W; Yoo B-W; Yoon CMSynthesis of Diethyl Pyridin-2-ylphosphonates and Quinolin-2-ylphosphonates by Deoxygenative Phosphorylation of the Corresponding N-Oxides. Bull. Korean Chem. Soc2014, 35, 2155–2158.

(72). Salaam J; Tabti L; Bahamyirou S; Lecointre A; Hernandez Alba O; Jeannin O; Camerel F; Cianférani S; Bentouhami E; Nonat AM; Charbonnière LJFormation of Mono- and Polynuclear Luminescent Lanthanide Complexes Based on the Coordination of Preorganized Phosphonated Pyridines. Inorg. Chem2018, 57, 6095–6106. [PubMed: 29746120]

(73). Hlinová V; Jaroš A; David T; Císařová I; Kotek J; Kubíček V; Hermann PComplexes of Phosphonate and Phosphinate Derivatives of Dipicolylamine. New J. Chem2018, 42, 7713–7722.

(74). Summers SP; Abboud KA; Farrah SR; Palenik GJSyntheses and Structures of Bismuth(III) Complexes with Nitrilotriacetic Acid, Ethylenediaminetetraacetic Acid, and Diethylenetriaminepentaacetic Acid. Inorg. Chem1994, 33, 88–92.

(75). Csajbók É; Baranyai Z; Bányai I; Brücher E; Király R; Müller-Fahrnow A; Platzek J; Radüchel B; Schäfer MEquilibrium, ^{1}H and ^{13}C NMR Spectroscopy, and X-Ray Diffraction Studies on the Complexes $Bi(DOTA)^{-}$ and Bi(DO3A-Bu). Inorg. Chem2003, 42, 2342–2349. [PubMed: 12665368]

(76). Shimoni-Livny L; Glusker JP; Bock CWLone Pair Functionality in Divalent Lead Compounds. Inorg. Chem1998, 37, 1853–1867.

(77). Llunell M; Casanova D; Cirera J; Alemany P; Alvarez SSHAPE 2.1University of Barcelona: Barcelona, Spain2013.

(78). Tao J; Perdew JP; Staroverov VN; Scuseria GEClimbing the Density Functional Ladder: Nonempirical Meta–Generalized Gradient Approximation Designed for Molecules and Solids. Phys. Rev. Lett2003, 91, 146401. [PubMed: 14611541]

(79). Metz B; Stoll H; Dolg MSmall-Core Multiconfiguration-Dirac-Hartree-Fock-Adjusted Pseudopotentials for Post-d Main Group Elements: Application to PbH and PbO. J. Chem. Phys2000, 113, 2563–2569.

(80). Schäfer A; Huber C; Ahlrichs RFully Optimized Contracted Gaussian Basis Sets of Triple Zeta Valence Quality for Atoms Li to Kr. J. Chem. Phys1994, 100, 5829–5835.

(81). Matito E; Solà MThe Role of Electronic Delocalization in Transition Metal Complexes from the Electron Localization Function and the Quantum Theory of Atoms in Molecules Viewpoints. Coord. Chem. Rev2009, 253, 647–665.

(82). Esteban-Gómez D; Platas-Iglesias C; Enríquez-Pérez T; Avecilla F; de Blas A; Rodríguez-Blas TLone-Pair Activity in Lead(II) Complexes with Unsymmetrical Lariat Ethers. Inorg. Chem2006, 45, 5407–5416. [PubMed: 16813404]

(83). Ferreirós-Martínez R; Esteban-Gómez D; de Blas A; Platas-Iglesias C; Rodríguez-Blas TEight-Coordinate Zn(II), Cd(II), and Pb(II) Complexes Based on a 1,7-Diaza-12-Crown-4 Platform Endowed with a Remarkable Selectivity over Ca(II). Inorg. Chem2009, 48, 11821–11831. [PubMed: 19911785]

(84). Baumann W; Schulz A; Villinger AA Blue Homoleptic Bismuth–Nitrogen Cation. Angew. Chem., Int. Ed2008, 47, 9530–9532.

(85). Bader RFWA Quantum Theory of Molecular Structure and Its Applications. Chem. Rev1991, 91, 893–928.

(86). Varadwaj PR; Marques HMThe Physical Chemistry of Coordinated Aqua-, Ammine-, and Mixed-Ligand Co^{2+} Complexes: DFT Studies on the Structure, Energetics, and Topological Properties of the Electron Density. Phys. Chem. Chem. Phys2010, 12, 2126–2138. [PubMed: 20165761]

(87). Varadwaj PR; Marques HMThe Physical Chemistry of $[M(H_2O)_4(NO_3)_2]$ (M = Mn^{2+}, Co^{2+}, Ni^{2+}, Cu^{2+}, Zn^{2+}) Complexes: Computational Studies of Their Structure, Energetics and the Topolog. Theor. Chem. Acc2010, 127, 711–725.

(88). Chauvin R; Lepetit C; Silvi B; Alikhani EApplications of Topological Methods in Molecular Chemistry; 2016.

(89). Mountain ARE; Kaltsoyannis NDo QTAIM Metrics Correlate with the Strength of Heavy Element-Ligand Bonds?Dalton Trans. 2013, 42, 13477–13486. [PubMed: 23897486]

(90). Dan D; Celis-Barros C; White FD; Sperling JM; Albrecht-Schmitt TEOrigin of Selectivity of a Triazinyl Ligand for Americium(III) over Neodymium(III). Chem. - Eur. J2019, 25, 3248–3252. [PubMed: 30716170]

(91). White FD; Gaiser AN; Warzecha EJ; Sperling JM; Celis-Barros C; Salpage SR; Zhou Y; Dilbeck T; Bretton AJ; Meeker DS; Hanson KG; Albrecht-Schmitt TEExamination of Structure and Bonding in 10-Coordinate Europium and Americium Terpyridyl Complexes. Inorg. Chem2018, 57, 12969–12975. [PubMed: 30265525]

(92). Windorff CJ; Celis-Barros C; Sperling JM; McKinnon NC; Albrecht-Schmitt TEProbing a Variation of the Inverse-Trans-Influence in Americium and Lanthanide Tribromide Tris(Tricyclohexylphosphine Oxide) Complexes. Chem. Sci2020, 11, 2770–2782. [PubMed: 34084337]

(93). Arnold PL; Prescimone A; Farnaby JH; Mansell SM; Parsons S; Kaltsoyannis NCharacterizing Pressure-Induced Uranium C-H Agostic Bonds. Angew. Chem., Int. Ed2015, 54, 6735–6739.

(94). Mansell SM; Kaltsoyannis N; Arnold PLSmall Molecule Activation by Uranium Tris(Aryloxides): Experimental and Computational Studies of Binding of N_2, Coupling of CO, and Deoxygenation Insertion of CO_2 under Ambient Conditions. J. Am. Chem. Soc2011, 133, 9036–9051. [PubMed: 21591662]

(95). Tassell MJ; Kaltsoyannis NCovalency in $AnCp_4$ (An = Th-Cm): A Comparison of Molecular Orbital, Natural Population and Atoms-in-Molecules Analyses. Dalton Trans. 2010, 39, 6719–6725. [PubMed: 20631951]

(96). Warzecha E; Celis-Barros C; Dilbeck T; Hanson K; Albrecht-Schmitt TEHigh-Pressure Studies of Cesium Uranyl Chloride. Inorg. Chem2019, 58, 228–233. [PubMed: 30569703]

(97). Chemey AT; Celis-Barros C; Huang K; Sperling JM; Windorff CJ; Baumbach RE; Graf DE; Páez-Hernández D; Ruf M; Hobart DE; Albrecht-Schmitt TEElectronic, Magnetic, and Theoretical Characterization of $(NH_4)_4UF_8$, a Simple Molecular Uranium(IV) Fluoride. Inorg. Chem2019, 58, 637–647. [PubMed: 30569705]

(98). Macchi P; Sironi AChemical Bonding in Transition Metal Carbonyl Clusters: Complementary Analysis of Theoretical and Experimental Electron Densities. Coord. Chem. Rev2003, 238–239, 383–412.

(99). Lindquist-Kleissler B; Wenger JS; Johnstone TCAnalysis of Oxygen-Pnictogen Bonding with Full Bond Path Topological Analysis of the Electron Density. Inorg. Chem2021, 60, 1846–1856. [PubMed: 33471517]

(100). Scherer W; Sirsch P; Grosche M; Spiegler M; Mason SA; Gardiner MGAgostic Deformations Based on Electron Delocalization in the Alkyllithium-Complex $[\{2\text{-}(Me_3Si)_2CLiC_5H_4N\}_2]$. Chem. Commun2001, 2072–2073.

(101). Scherer W; Sirsch P; Shorokhov D; McGrady GS; Mason SA; Gardiner MGValence-Shell Charge Concentrations and Electron Delocalization in Alkyllithium Complexes: Negative Hyperconjugation and Agostic Bonding. Chem. - Eur. J2002, 8, 2324–2334. [PubMed: 12012416]

(102). Tafipolsky M; Scherer W; Öfele K; Artus G; Pedersen B; Herrmann WA; McGrady GS; Herrmann A, W.; Sean McGrady GElectron Delocalization in Acyclic and *N*-Heterocyclic Carbenes and Their Complexes: A Combined Experimental and Theoretical Charge-Density Study. J. Am. Chem. Soc2002, 124, 5865–5880. [PubMed: 12010062]

(103). Ott H; Däschlein C; Leusser D; Schildbach D; Seibel T; Stalke D; Strohmann CStructure/ Reactivity Studies on an α-Lithiated Benzylsilane: Chemical Interpretation of Experimental Charge Density. J. Am. Chem. Soc2008, 130, 11901–11911. [PubMed: 18702464]

(104). Espinosa Ferao A; García Alcaraz A; Zaragoza Noguera S; Streubel RTerminal Phosphinidene Complex Adducts with Neutral and Anionic O-Donors and Halides and the Search for a Differentiating Bonding Descriptor. Inorg. Chem2020, 59, 12829–12841. [PubMed: 32805993]

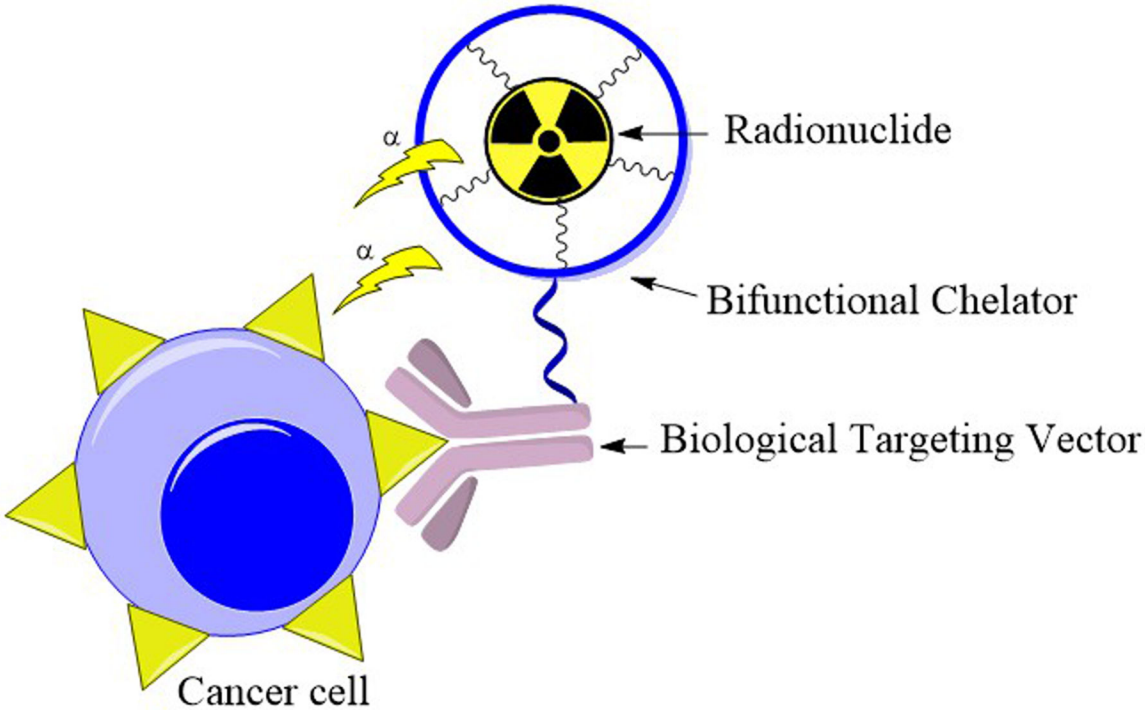

Figure 1.
Schematic of TAT, demonstrating the role of the BFC in bridging the radiometal to the biological targeting vector.

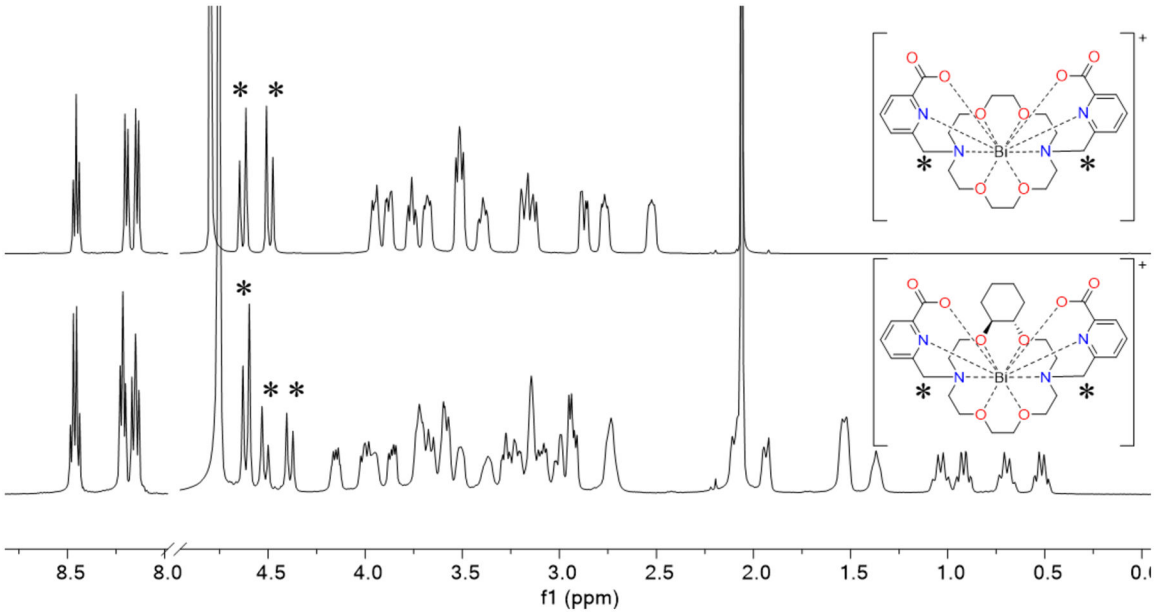

Figure 2.

^{1}H NMR spectra (500 MHz, 298 K, D_2O) of $[Bi(macropa)]^+$ (top) and $[Bi(CHX\text{-}macropa)]^+$ (bottom), demonstrating C_2 or C_1 symmetry, respectively. The diagnostic aliphatic resonances marked by asterisks for each corresponds to the similarly marked methylene arm linker protons.

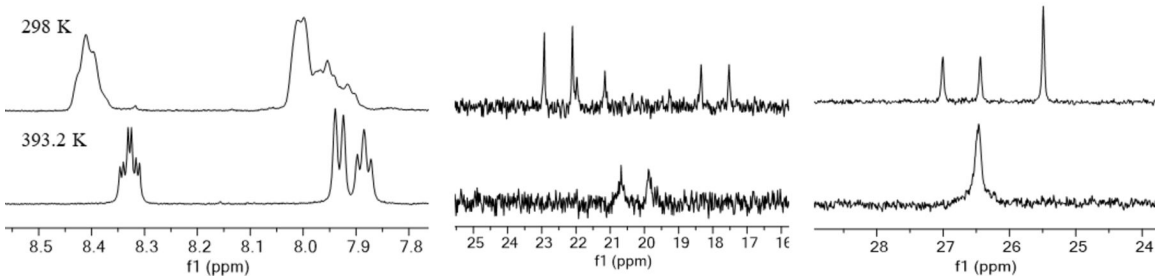

Figure 3.

^{1}H (left, 500 MHz), ^{13}C{^{1}H} (middle, 126 MHz), and ^{31}P{^{1}H} (right, 202 MHz) NMR spectra of [Bi(macrophosphi)]$^{+}$ in DMSO-d_6 at 298 K (top) and 393.2 K (bottom).

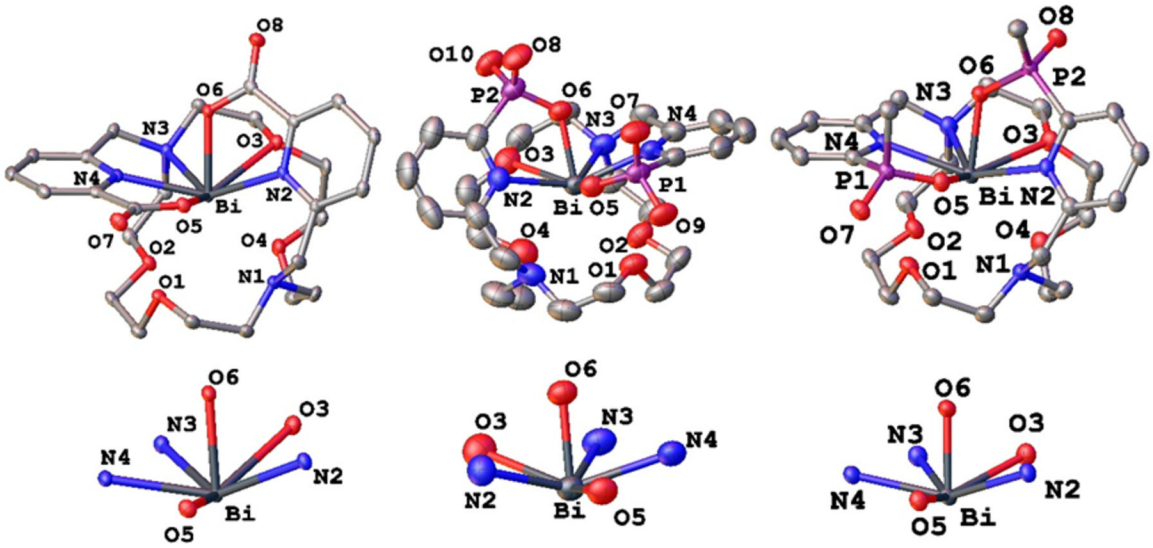

Figure 4.

X-ray crystal structures of [Bi(macropa)](NO_3)·dioxane (top left), [Bi(macrophospho)](TFA)·H_2O (top middle), and [Bi(macrophosphi)](TFA)·H_2O (top right) complexes. Ellipsoids are drawn at the 50% probability level. Hydrogen atoms, counteranions, and solvent molecules are excluded for clarity. The six donor atoms that comprise the pentagonal pyramidal coordination sphere of the Bi^{3+} are shown below each structure.

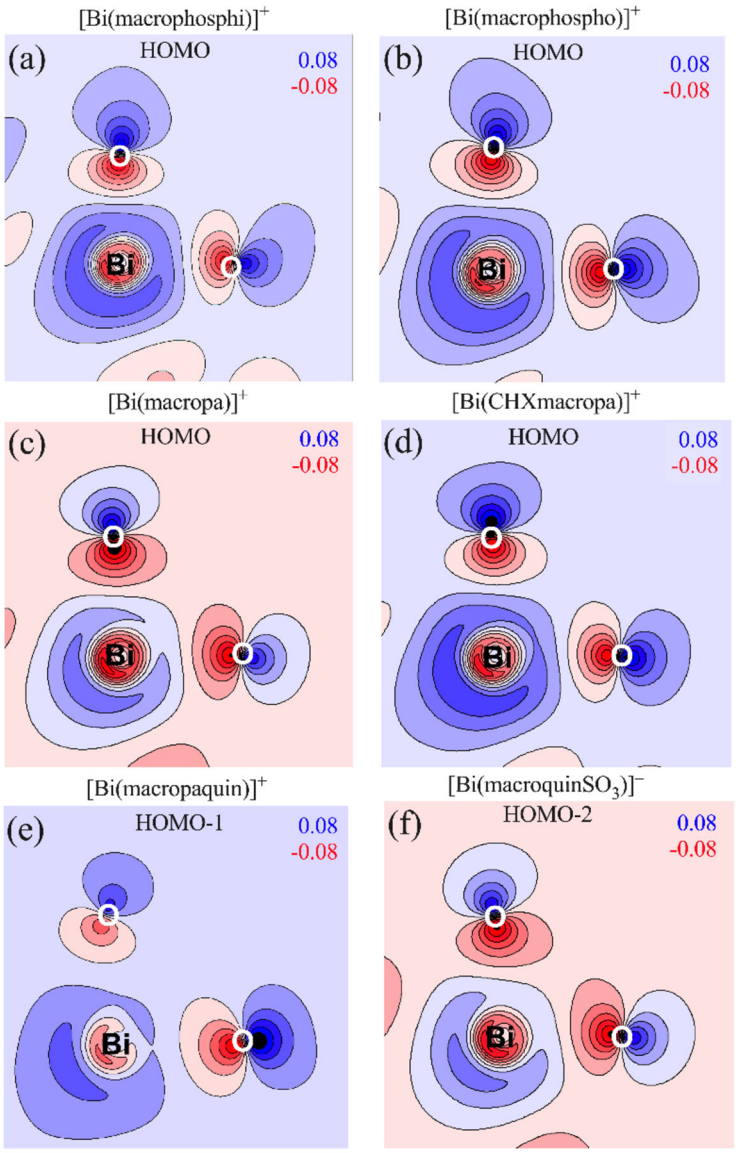

Figure 5.

Contour plots of the electron density (e^{-} $Å^{-3}$) for the MOs containing significant Bi $6s^2$ contribution on the plane defined by the Bi^{3+} ion and the oxygen donor atoms of the pendent arms. (A) $[Bi(macrophosphi)]^{+}$ HOMO, (B) $[Bi(macrophospho)]^{+}$ HOMO, (C) $[Bi(macropa)]^{+}$ HOMO, (D) $[Bi(CHX\text{-}macropa)]^{+}$ HOMO, (E) $[Bi(macropaquin)]^{+}$ HOMO–1, (F) $[Bi(macroquin\text{-}SO_3)]^{-}$ HOMO–2. Values indicate maximum (blue) and minimum (red) electron density isovalues.

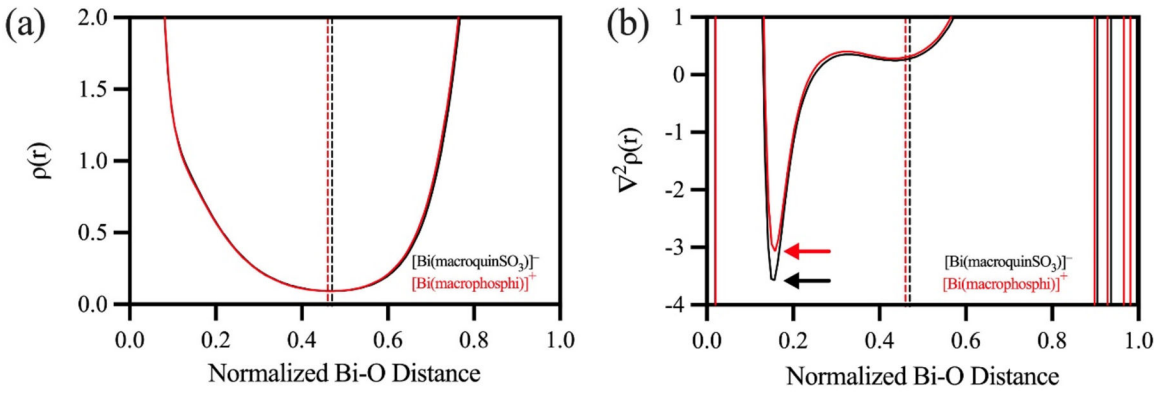

Figure 6.

Evaluation of (a) ρ and (b) $\nabla^2\rho$ along the normalized Bi–O bond paths of $[Bi(macrophosphi)]^+$ and $[Bi(macroquin\text{-}SO_3)]^-$. Dashed vertical lines represent the location of the BCP.

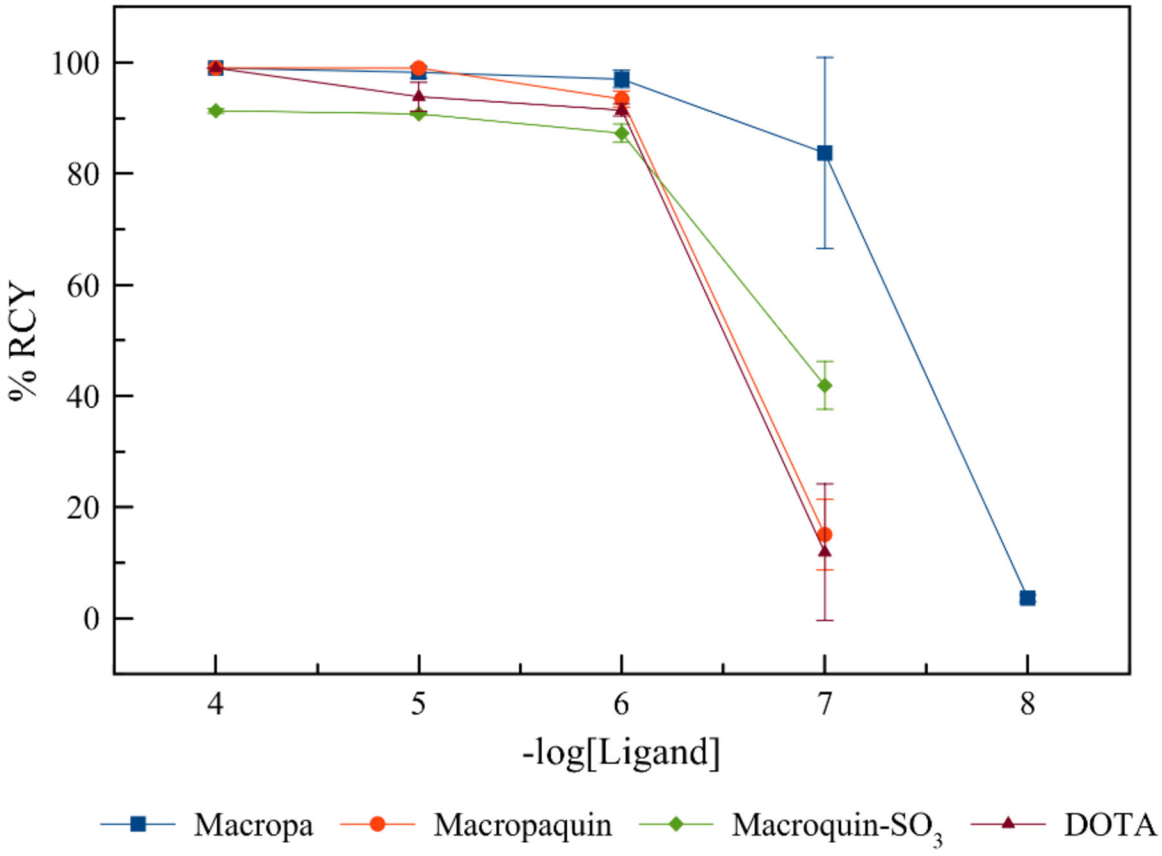

Figure 7.

RCYs for each ligand vs. concentration. Concentration-dependent radiolabeling studies were performed by the addition of $[^{213}Bi]BiI_4^-$/$[^{213}Bi]BiI_5^{2-}$ (30 kBq–210 kBq) to a solution containing ligands in MES buffer (0.5 M, pH 5.5–6). All radiolabeling studies were carried out within 5 min post-elution of the $^{225}Ac/^{213}Bi$ generator. Macropa, macropaquin, and macroquin-SO_3 were incubated at room temperature for 8 min, whereas DOTA was incubated at 95 °C for 5.5 min.

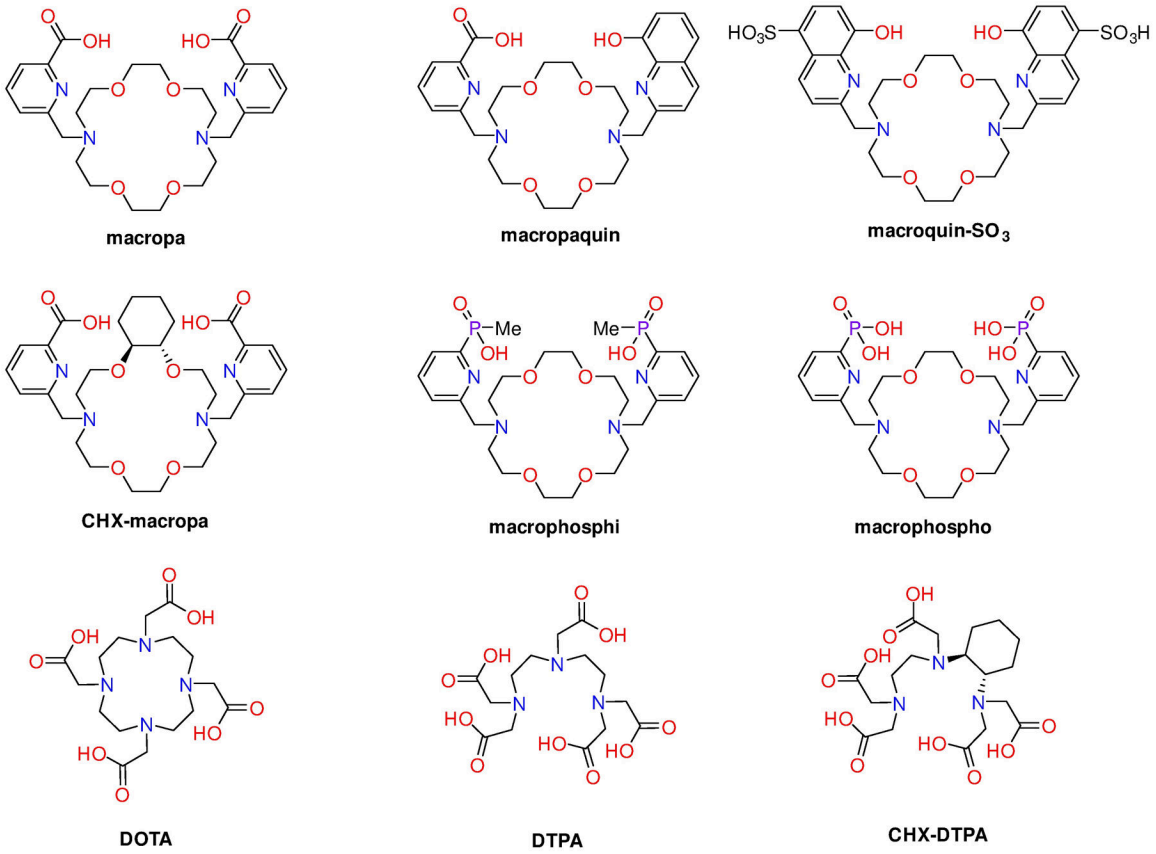

Chart 1.
Ligands discussed in this work.

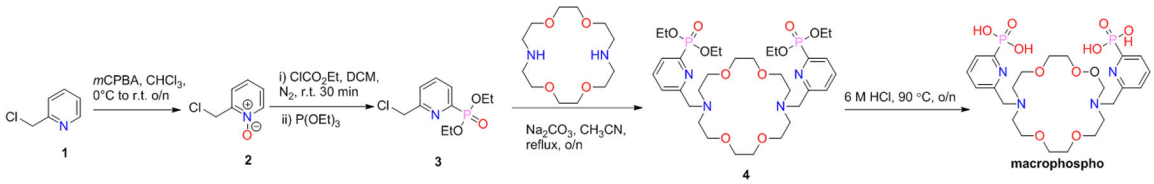

Scheme 1.
Synthesis of macrophospho

Table 1.

Protonation Constants for Investigated Ligands Determined via pH Potentiometry (25 °C and I = 0.1 M KCl)

	macropa^{2-} [a]	**macropaquin^{2-}** [b]	**macroquin-SO$_3^{4-}$** [b]	**CHX-macropa^{2-}** [c]	**macrophosphi^{2-}** [d]	**macrophospho^{2-}**
log K_{a1}	7.41	10.33	9.34	7.77	8.13	8.68(1)
log K_{a2}	6.85	7.15	9.43	6.95	6.77	7.82(1)
log K_{a3}	3.32	6.97	6.75	3.17	1.97	6.37(1)
log K_{a4}	2.36	3.24	6.62	2.51		5.68(1)
log K_{a5}	1.69					1.50(6)

[a] Reference 58,

[b] Reference 59,

[c] Reference 60,

[d] Reference 69

Table 2.

Interatomic Distances (Å) Involving Bi[a]

Bond	[Bi(macropa)]$^+$	[Bi(macrophospho)]$^+$	[Bi(macrophosphi)]$^+$
Bi–O1	2.987(2)	2.960(3)	2.909(2)
Bi–O2	2.895(2)	2.934(4)	2.868(2)
Bi–O3	2.7541(17)	2.740(4)	2.669(2)
Bi–O4	3.048(2)	3.259(4)	3.257(3)
Bi–O5	2.2577(16)	2.232(3)	2.254(2)
Bi–O6	2.2316(17)	2.212(3)	2.216(2)
Bi–N1	2.930(3)	2.992(5)	3.014(4)
Bi–N2	2.4419(19)	2.538(4)	2.566(3)
Bi–N3	2.688(2)	2.666(4)	2.659(3)
Bi–N4	2.413(2)	2.434(4)	2.442(3)

[a]Atoms are labeled as shown in Figure 4. The values in the parentheses are one standard deviation of the last significant figure(s).

Table 3.

Half-Lives of Bi^{3+} Complexes in the Presence of 1000× Excess DTPA at pH 7.4.

Complex	Half-life
$[Bi(macrophosphi)]^{+}$	< 1 min
$[Bi(macrophopho)]^{+}$	8.9 ± 1.7 min
$[Bi(CHX\text{-}macropa)]^{+}$	40.4 ± 4.3 min
$[Bi(macropa)]^{+}$	46.6 ± 0.9 min
$[Bi(macropaquin)]^{+}$	14.3 ± 1.4 h
$[Bi(macroquin\text{-}SO_3)]^{-}$	> 21 d

Table 4.

NBO Analysis of the Bi^{3+} Lone Pair for $[Bi(L)]^{+/-}$ Complexes

Complex	
$[Bi(macrophosphi)]^{+}$	s(98.79%) p(1.20%)
$[Bi(macrophospho)]^{+}$	s(98.74%) p(1.26%)
$[Bi(CHX\text{-}macropa)]^{+}$	s(98.14%) p(1.85%)
$[Bi(macropa)]^{+}$	s(98.10%) p(1.89%)
$[Bi(macropaquin)]^{+}$	s(98.05%) p(1.95%)
$[Bi(macroquin\text{-}SO_3)]^{-}$	s(98.19%) p(1.80%)

Table 5.

Selected QTAIM Metrics for Bi–Donor Interactions with the Ligand Pendent Arms in $[Bi(L)]^{+/-}$ Complexes. The Corresponding Units are ρ (e^{-} $Å^{-3}$), H/ρ (kJ/mol per e^{-}), |V|/G (unitless), and δ (unitless)

Complex	ρ(r)		H/ρ		|V|/G		δ	
	Bi–O6[a]	Bi–O5	Bi–O6	Bi–O5	Bi–O6	Bi–O5	Bi–O6	Bi–O5
[Bi(macrophosphi)]$^{+}$	0.0790	0.0816	−481.7647	−500.7658	1.1599	1.1648	0.9476	0.9708
[Bi(macrophospho)]$^{+}$	0.0718	0.0881	−432.9824	−540.2123	1.1495	1.1707	0.8771	0.9977
[Bi(CHX-macropa)]$^{+}$	0.0786	0.0776	−502.2058	−498.0826	1.1729	1.1724	0.9626	0.9523
[Bi(macropa)]$^{+}$	0.0778	0.0792	−498.4372	−506.3900	1.1724	1.1737	0.9526	0.9690
[Bi(macropaquin)]$^{+}$	0.0790	0.0797	−503.1691	−524.1951	1.1726	1.1820	0.9715	0.9831
[Bi(macroquinSO_3)]$^{-}$	0.0872	0.0872	−579.2422	−579.2698	1.2008	1.2008	1.0345	1.0345
Complex	**ρ(r)**		**H/ρ**		**|V|/G**		**δ**	
	Bi–N2	**Bi–N4**	**Bi–N2**	**Bi–N4**	**Bi–N2**	**Bi–N4**	**Bi–N2**	**Bi–N4**
[Bi(macrophosphi)]$^{+}$	0.0507	0.0416	−350.5292	−261.7623	1.1785	1.1398	0.6846	0.6054
[Bi(macrophospho)]$^{+}$	0.0476	0.0444	−321.6876	−291.0008	1.1654	1.1527	0.6499	0.6323
[Bi(CHX-macropa)]$^{+}$	0.0155	0.0322	234.3138	−206.1312	0.8699	1.1323	0.2722	0.4715
[Bi(macropa)]$^{+}$	0.0566	0.0512	−401.4145	−353.3262	1.1957	1.1766	0.7238	0.6839
[Bi(macropaquin)]$^{+}$	0.0152	0.0263	301.8964	−86.6741	0.8457	1.0523	0.2916	0.4341
[Bi(macroquinSO_3)]$^{-}$	0.0581	0.0581	−407.7068	−407.6882	1.2066	1.2066	0.7213	0.7213

[a]Atom numbering scheme is shown in Figure S48.

Table 6.

Average RCYs (%) of [^{213}Bi]Bi-Complexes at 95 °C for DOTA after 5.5 min and Room Temperature for other Ligands after 8 min

Ligand Concentration	macropa	macropaquin	macroquin-SO_3	DOTA (95 °C)
10^{-4} M	>99	>99	91 ± 1	>99
10^{-5} M	98 ± 1	>99	91 ± 1	94 ± 3
10^{-6} M	97 ± 2	93 ± 2	87 ± 2	91 ± 1
10^{-7} M	84 ± 17	15 ± 6	42 ± 4	12 ± 12
10^{-8}M	4 ± 1			

Table 7.

Molar Activities (MBq/nmol) of [^{213}Bi]Bi-Complexes at the Lowest Ligand Concentrations Required to Attain > 80% RCY

Ligand	Molar Activity (MBq/nmol)
macropa	8.69
macropaquin	1.49
macroquin-SO_3	1.82
DOTA	0.284